The molecular structure of the mineral sarmientite $Fe_2(AsO_4,SO_4)_2(OH)_6{\cdot}5H_2O$ –implications for arsenic accumulation and removal

Ray L. Frost,• Sara J. Palmer, Yunfei Xi

Chemistry Discipline, Faculty of Science and Technology, Queensland University of Technology, GPO Box 2434, Brisbane Queensland 4001, Australia.

ABSTRACT

Sarmientite is an environmental mineral; its formation in soils enables the entrapment and immobilisation of arsenic. The mineral sarmientite is often amorphous making the application of X-ray diffraction difficult. Vibrational spectroscopy has been applied to the study of sarmientite. Bands are attributed to the vibrational units of arsenate, sulphate, hydroxyl and water.

Raman bands at 794, 814 and 831 cm^{-1} are assigned to the ν_3 $(AsO_4)^{3-}$ antisymmetric stretching modes and the ν_1 symmetric stretching mode is observed at 891 cm^{-1}. Raman bands at 1003 and 1106 cm^{-1} are attributed to SO_4^{2-} vibrations. The Raman band at 484 cm^{-1} is assigned to the triply degenerate $(AsO_4)^{3-}$ bending vibration. The high intensity Raman band observed at 355 cm^{-1} (both lower and upper) is considered to be due to the $(AsO_4)^{3-}$ ν_2 bending vibration. Bands attribute to water and OH stretching vibrations are observed.

KEYWORDS: sarmientite, arsenate, arsenic removal, sulphate, Raman spectroscopy

• Author to whom correspondence should be addressed (r.frost@qut.edu.au)

Introduction

The mineral sarmientite $Fe_2(AsO_4,SO_4)_2(OH)_6 \cdot 5H_2O$ [1] is a mineral containing three anions namely sulphate, arsenate and hydroxyl. The mineral is monoclinic of point group 2/m. The crystals are prismatic and are aggregated into nodules [2]. The mineral was discovered in 1941 [3] and the single crystal X-ray study [1] yields the unit cell data: a 6.55, b 18.55, c 9.70 Å, β 97°39', P21/c, Z = 4, d =2.58. The mineral is analogous to the mineral destinezite. The mineral destinezite is a hydrated hydroxy phosphate of ferric iron with some sulphate substitution of formula $Fe_2(PO_4,SO_4)_2(OH) \cdot 6H_2O$ with the iron in the ferric state [4-7]. According to Peacor *et al.* [6] the crystal structure consists of infinite chains of $Fe(O,OH,H_2O)_6$ octahedra, sulphate tetrahedra and phosphate tetrahedra linked by a unique system of vertex sharing. The chains are weakly bonded into layers by hydrogen bonding between OH and H_2O of the Fe(III) octahedra and oxygen ions of the sulphate tetrahedra [6]. Layers of tetrahedral/octahedral chains alternate with sheets of H_2O molecules. Peacor *et al.* [6] stated that the structure resembles hydrated clay minerals, with H_2O molecules that act as hydrogen bond donors and acceptors to oxygen atoms of adjacent slabs. The mineral has a clay-like appearance under the SEM. The amorphous form of the sarmientite mineral is an example of a colloidal mineral [5, 8-10]. These minerals are X-ray non-diffracting and so vibrational spectroscopy is very important for the characterisation of this mineral and forms the objective of this research.

Sarmientite can be described as an environmental mineral in that its formation, for example in soils, enables the entrapment and immobilisation of arsenic [11, 12]. This mineral is essential for the formation of compounds containing arsenic [13-15]. It is formed in old mine sites and slag piles [14-16]. Complex equilibria exist with the formation of the mineral which may redissolve in heavy rainfall events [14]. Such mineral formation can be made to control the concentrations of lead and arsenic in mine tailings [17]. Arsenate is accumulated in the formation of secondary minerals in the beudantite-jarosite mineral groups [13]. The formation of secondary arsenate containing minerals is extremely important in the accumulation and immobilization of arsenic and heavy metals [18]. Of course other minerals such as segnitite, jarosite, bukovskýite may also function as metal collectors. Such mineral formation will depend upon the conditions of formation and the associated equilibria. The reason for this research is that minerals such as sarmientite are found in soils and in old mine

sites. Further, the formation of such a mineral can be used as the basis for arsenic accumulation. Therefore, this research focuses on the molecular structure of sarmientite.

Raman spectroscopy has proven very useful for the study of minerals. Indeed Raman spectroscopy has proven most useful for the study of diagenetically related minerals as often occurs with minerals containing sulphate and arsenate groups, including sarmientite, beudantite and bukovskyite. Raman spectroscopy is especially useful when the minerals are X-ray non-diffracting or poorly diffracting and very useful for the study of amorphous and colloidal minerals as is the case for sarmientite. This paper is a part of systematic studies of vibrational spectra of minerals of secondary origin in the oxide supergene zone. In this work we attribute bands at various wavenumbers to vibrational modes of sarmientite using Raman spectroscopy and relate the spectra to the structure of the mineral.

Experimental

Mineral

The mineral sarmientite samples were supplied by The Mineralogical Research Company. The minerals originated from Bou Azzer, Tazenakht, Ouarzazate Province, Souss-Massa-Draa Region, Morocco. The mineral data has been published (page 522) [2].

Raman spectroscopy

Crystals of sarmientite were placed on a polished metal surface on the stage of an Olympus BHSM microscope, which is equipped with 10x, 20x, and 50x objectives. The microscope is part of a Renishaw 1000 Raman microscope system, which also includes a monochromator, a filter system and a CCD detector (1024 pixels). The Raman spectra were excited by a Spectra-Physics model 127 He-Ne laser producing highly polarised light at 633 nm and collected at a nominal resolution of 2 cm^{-1} and a precision of ± 1 cm^{-1} in the range between 100 and 4000 cm^{-1}. Repeated acquisition on the crystals using the highest magnification (50x) were accumulated to improve the signal to noise ratio in the spectra. Spectra were calibrated using the 520.5 cm^{-1} line of a silicon wafer. Further details of the technique have been published [19-25].

Infrared spectroscopy

Infrared spectra were obtained using a Nicolet Nexus 870 FTIR spectrometer with a smart endurance single bounce diamond ATR cell. Spectra over the 4000–525 cm^{-1} range were obtained by the co-addition of 128 scans with a resolution of 4 cm^{-1} and a mirror velocity of 0.6329 cm/s. Spectra were co-added to improve the signal to noise ratio.

Band component analysis was undertaken using the Jandel 'Peakfit' (Erkrath, Germany) software package which enabled the type of fitting function to be selected and allowed specific parameters to be fixed or varied accordingly. Band fitting was done using a Lorentz-Gauss cross-product function with the minimum number of component bands used for the fitting process. The Lorentz-Gauss ratio was maintained at values greater than 0.7 and fitting was undertaken until reproducible results were obtained with squared correlations (r^2) greater than 0.995. Band fitting of the spectra is quite reliable providing there is some band separation or changes in the spectral profile.

RESULTS and DISCUSSION

Background

S.D. Ross in Farmer's treatise [26] reported the infrared spectrum of beudantite (Table 18.IX page 433). The spectroscopy of beudantite should be close to that of sarmientite. This table compares the infrared spectra of minerals from the alunite-jarosite supergroups. Ross reported infrared bands at 985, 1006 cm^{-1} (ν_1), 430, 466 cm^{-1} (ν_2), 1078, 1160 cm^{-1} (ν_3), 600, 625 and 670 cm^{-1} (ν_4). OH vibrations were reported at 3420 and 525 cm^{-1} attributed to the stretching and bending of the OH units. Sejkora *et al*. [27] published the infrared spectrum of a copper rich beudantite and found OH stretching vibrations at 2924, 3208 and 3362 cm^{-1} and assigned these bands to hydrogen bonded non-equivalent OH units in the beudantite structure. The sulphate stretching mode for the Cu-beudantite [27] was listed as 1010 cm^{-1} and the ν_2 bending modes at 620, 662 and 687 cm^{-1}. The arsenate stretching bands were listed as occurring at 729, 813, 821, 851 and 870 cm^{-1}. The arsenate bending modes were not reported, no doubt because these bands occur outside the detection limits of the instrument.

Spectroscopy

The Raman and infrared spectra of sarmientite over the complete spectral range is displayed in Figures 1 and 2 respectively. These figures show the relative intensities of the bands both within each spectrum and between the two vibrational spectra. The bands associated with the OH stretching vibrations show significantly more intensity in the infrared spectrum. The spectra show the relative intensities of the bands in each of the spectral regions. The Raman spectrum of sarmientite in the 700 to 950 cm^{-1} region is reported in Figure 3. This spectral region reports the stretching region of the arsenate anion. The intensities of the two samples vary but in terms of band positions the spectra are identical. The difference between the two spectra is probably due to orientation effects. In the bottom spectrum, the band at 893 cm^{-1} is assigned to the ν_1 symmetric stretching mode. In the top spectrum, the band is observed at 891 cm^{-1}. The overlapping set of bands at 794, 814 and 831 cm^{-1} are assigned to the ν_3 antisymmetric stretching modes. Raman bands in the upper spectrum are found at 788, 823, 836 and 855 cm^{-1}. The bands at 719 and 750 cm^{-1} may be attributed to OH deformation modes.

The infrared spectrum of sarmientite over the 575 to 875 cm^{-1} range is shown in Figure 4. The spectral profile consists of a set of overlapping bands which may be resolved into component bands. The infrared band at 831 cm^{-1} in the lower spectrum and the band at 824 cm^{-1} in the upper spectrum is probably the infrared equivalent of the symmetric stretching mode. The infrared bands at 746, 776 and 799 cm^{-} (lower spectrum) and 750, 777 and 798 cm^{-1} (upper) are assigned to the ν_3 antisymmetric stretching modes.

The Raman spectra of the 950 to 1250 cm^{-1} region are shown in Figure 5. Differences are observed between the spectra of the two samples. The band at 1003 cm^{-1} (lower spectrum) is assigned to the SO_4^{2-} symmetric stretching band. The bands at 1106 are attributed to the SO_4^{2-} antisymmetric stretching vibration. The bands at 1607 cm^{-1} (lower) and 1602 cm^{-1} (upper) are assigned to the water bending modes. It is not known what is the origin of the other bands in the spectrum.

The infrared spectra in the 875 to 1375 cm^{-1} region are shown in Figure 6. The spectra display a complex set of overlapping bands which may be resolved into component bands. Strong infrared bands observed at 990 cm^{-1} (lower); and 991 and 1019 cm^{-1} (upper) are attributed to the SO_4^{2-} symmetric stretching modes. Infrared bands at 1053, 1087, 1122, 1167

and 1192 cm^{-1} (lower) and at 1050, 1085, 11189, 1118 and 1166 cm^{-1} (upper) are attributed to the SO_4^{2-} antisymmetric stretching vibrations.

The Raman spectra of beudantite in the 350 to 700 cm^{-1} region are displayed in Figure 7. The Raman spectra in this spectral range are very similar. This spectral region is where the sulphate bending vibrations are observed. The Raman bands at 528, 548, 592, 611 and 625 cm^{-1} (lower), 525, 544, 592, 625, and 639 cm^{-1} (upper), are assigned to the ν_4 $(SO_4)^{2-}$ bending modes. The infrared spectra of the studied samples in this spectral region are shown in Figure 4. Low intensity infrared bands are observed at 599 and 609 cm^{-1} (lower) and 581, 594 and 627 cm^{-1} (upper). These bands are the equivalent of the Raman bands and are attributed to the ν_4 $(SO_4)^{2-}$ bending modes.

In the infrared spectrum of beudantite, reported by Farmer [26], ν_2 modes were determined at 430 and 466 cm^{-1}. However, the exact assignment of these bands was not given. The Raman band at 484 cm^{-1} (Figure 8) is ascribed to the triply degenerate $(AsO_4)^{3-}$ bending vibration (F_2, ν_4). The Raman bands at 388 cm^{-1} with a shoulder at 404 cm^{-1} (lower), 395 and 404 cm^{-1} (upper) are assigned to the ν_2 $(SO_4)^{2-}$ bending mode. The high intensity Raman band observed at 355 cm^{-1} (both lower and upper) is considered to be due to the $(AsO_4)^{3-}$ ν_2 bending vibration. A series of far low wavenumber bands are observed for sarmientite in the 75 to 375 cm^{-1} region as is displayed in Figure 9. These bands may be described as lattice bands.

The Raman spectra in the OH stretching region are reported in Figure 10. The spectra are of low intensity and suffer from a lack of signal to noise. Raman bands are observed at around 2864, 2919, and 3340 cm^{-1}. The first two bands may be assigned to organic CH vibrations. The bands at 3340 cm^{-1} (lower) and at 3289, 3335, 3379 cm^{-1} (upper) are ascribed to water stretching vibrations. Such bands are inherently of low intensity because water is a very poor Raman scatterer. The infrared spectra of the OH stretching region are shown in Figure 11. A complex spectral profile is observed and component bands may be resolved based upon the inflections in the spectrum. Infrared bands are observed at 2925, 3193, 3409 and 3544 cm^{-1} (lower), and 2737, 2993, 3124, 3344 and 3514 cm^{-1}. These bands are attributed to hydroxyl unit stretching and water stretching vibrations. The sharp infrared band at 3514 cm^{-1} is assigned to the stretching vibrations of the hydroxyl units.

Conclusions

Raman and infrared spectroscopy has been used to study the molecular structure of sarmientite, a colloidal mineral often found in soils. The mineral is analogous to the mineral destinezite $Fe_2(PO_4,SO_4)_2(OH)\cdot 6H_2O$. The formation of sarmientite offers a mechanism for the uptake of arsenic from the environment.

Acknowledgements

The financial and infra-structure support of the Chemistry Discipline of the Faculty of Science and Technology, Queensland University of Technology is gratefully acknowledged. The Australian Research Council (ARC) is thanked for funding the instrumentation.

References

[1] M.E. Simenez de Abeledo, M.A.R. De Benyacar, American Mineralogist 53 (1968) 2077.
[2] J.W. Anthony, R.A. Bideaux, K.W. Bladh, M.C. Nichols, Handbook of Mineralogy Vol.IV. Arsenates, phosphates, vanadates - Mineral Data Publishing, Tucson, Arizona. Mineral data Publishing, Tucson, Arizona, 2000.
[3] V. Angelelli, S.G. Gordon, Notulae Naturae, Acad. Nat. Sci. Phila. (1941) 4 pp.
[4] V. Bouska, E.K. Lazarenko, Y.M. Melnik, E. Slanski, Acta Univ. Carolinae, Geol. (1960) 127.
[5] L.D. German, Zapiski Vserossiiskogo Mineralogicheskogo Obshchestva 85 (1956) 574.
[6] D.R. Peacor, R.C. Rouse, T.D. Coskren, E.J. Essene, Clays and Clay Minerals 47 (1999) 1.
[7] R. Sitzia, Rendiconti del Seminario della Facolta di Scienze dell'Universita di Cagliari 36 (1966) 105.
[8] M. Foldvari, B. Nagy, Foldtani Kozlony 115 (1985) 123.
[9] M.Z. Fursova, Izvestiya Akademii Nauk Kazakhskoi SSR, Seriya Geologicheskaya 22 (1965) 74.
[10] A.I. Ginzburg, Trudy Mineralogicheskogo Muzeya, Akademiya Nauk SSSR (1952) 36.
[11] K.Y. Chiang, K.C. Lin, S.C. Lin, T.-K. Chang, M.K. Wang, Journal of Hazardous Materials 181 (2010) 1066.
[12] A. Courtin-Nomade, C. Neel, H. Bril, M. Davranche, Bulletin de la Societe Geologique de France 173 (2002) 479.
[13] R. Giere, N.V. Sidenko, E.V. Lazareva, Applied Geochemistry 18 (2003) 1347.
[14] D.L. Harris, B.G. Lottermoser, J. Duchesne, Australian Journal of Earth Sciences 50 (2003) 797.
[15] F.M. Romero, R.M. Prol-Ledesma, C. Canet, L.N. Alvares, R. Perez-Vazquez, Applied Geochemistry 25 (2010) 716.
[16] C. Rewitzer, R. Hochleitner, Rivista Mineralogica Italiana (1989) 83.
[17] C. Roussel, C. Neel, H. Bril, Science of the Total Environment 263 (2000) 209.
[18] J.M. Nieto, M.A. Capitan, R. Saez, G.R. Almodovar, Transactions of the Institutions of Mining and Metallurgy, Section B: Applied Earth Science 112 (2003) B293.
[19] R.L. Frost, S. Bahfenne, J. Raman Spectrosc. 41 (2010) 207.
[20] R.L. Frost, S. Bahfenne, J. Raman Spectrosc. 41 (2010) 325.
[21] R.L. Frost, S. Bahfenne, J. Cejka, J. Sejkora, S.J. Palmer, R. Skoda, J. Raman Spectrosc. 41 (2010) 690.
[22] R.L. Frost, S. Bahfenne, J. Cejka, J. Sejkora, J. Plasil, S.J. Palmer, J. Raman Spectrosc. 41 (2010) 814.
[23] R.L. Frost, K.H. Bakon, S.J. Palmer, J. Raman Spectrosc. 41 (2010) 78.
[24] R.L. Frost, J. Cejka, J. Sejkora, J. Plasil, S. Bahfenne, S.J. Palmer, J. Raman Spectrosc. 41 (2010) 571.
[25] R.L. Frost, J. Cejka, J. Sejkora, J. Plasil, S. Bahfenne, S.J. Palmer, J. Raman Spectrosc. 41 (2010) 566.
[26] V.C. Farmer, Mineralogical Society Monograph 4: The Infrared Spectra of Minerals. 1974.
[27] J. Sejkora, J. Skovira, J. Cejka, J. Plasil, Journal of Geosciences 54 (2009) 355.

252
253

List of Figures

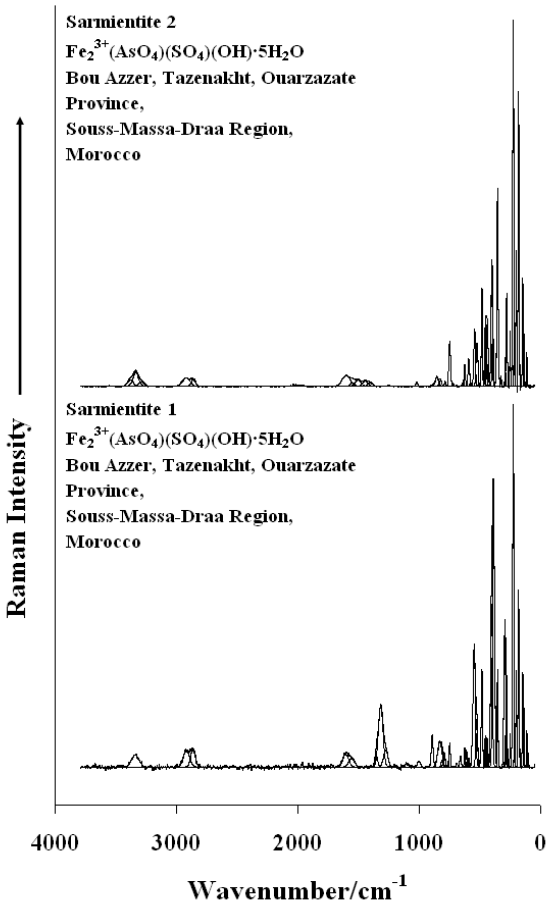

280

281

282 **Figure 1**

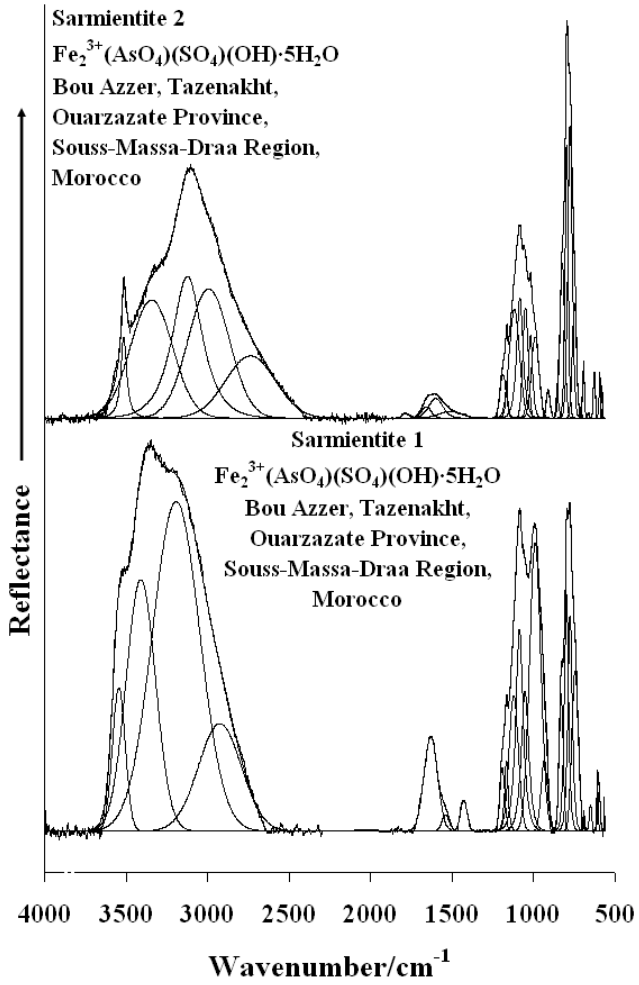

283

284

285 **Figure 2**

286

287

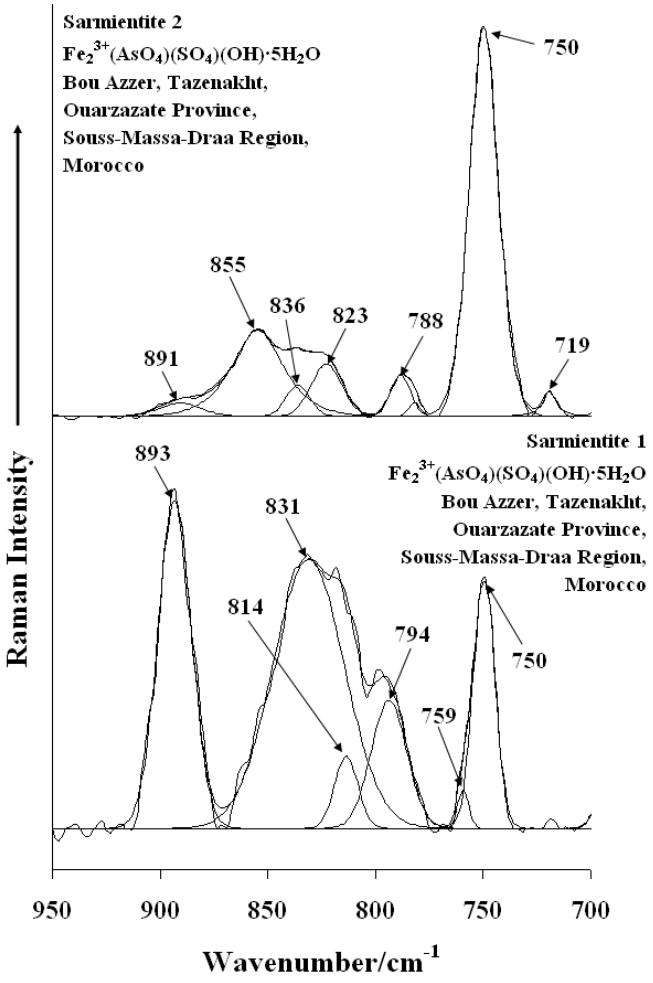

288

289

290 **Figure 3**

291

292

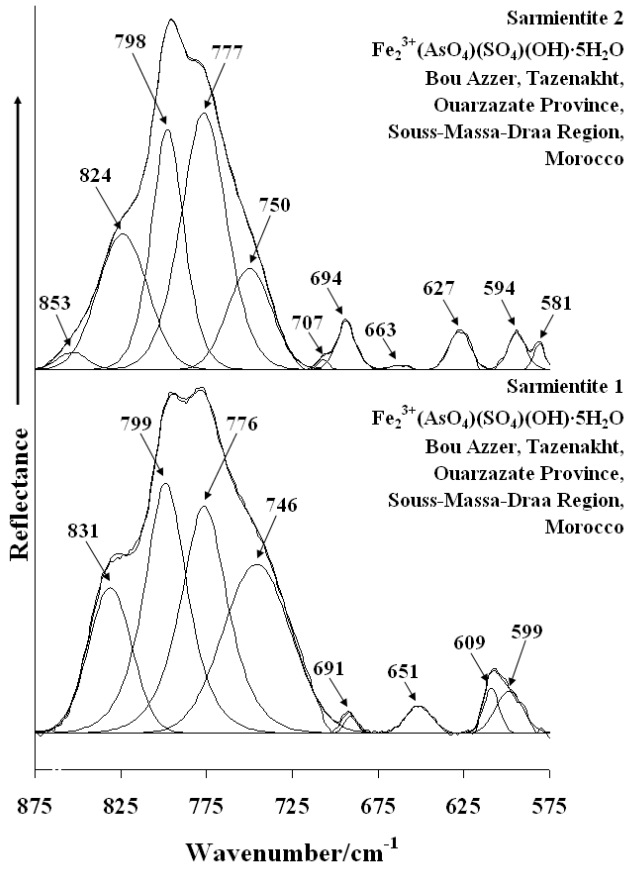

293

294

295

296 **Figure 4**

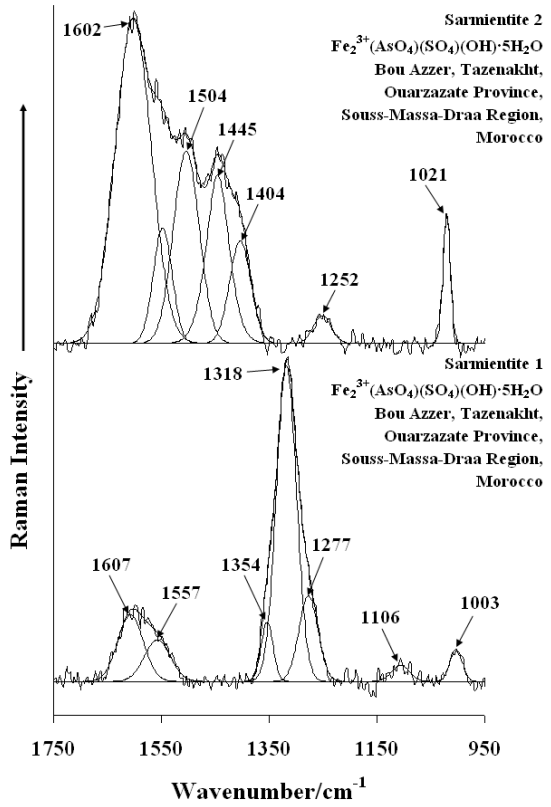

297

298

299 **Figure 5**

300

301

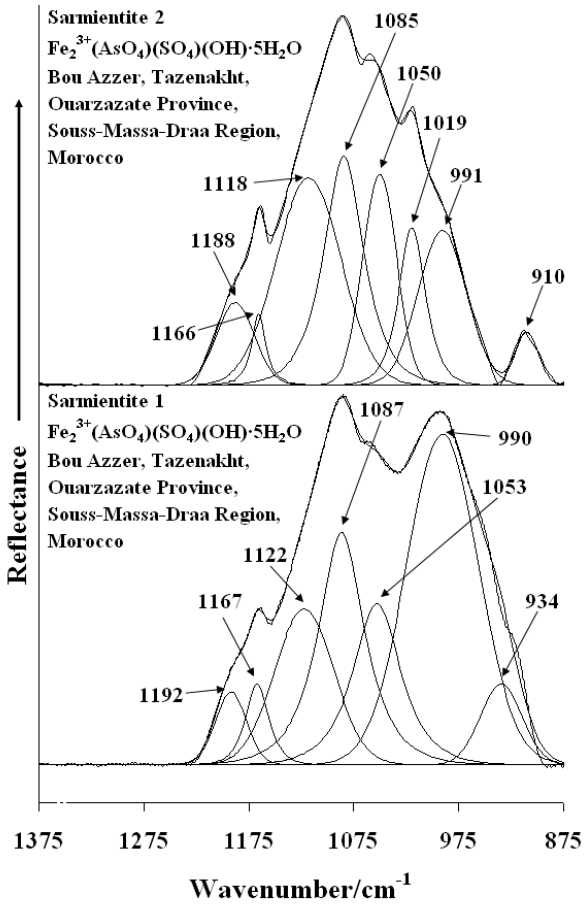

302

303

304 **Figure 6**

305

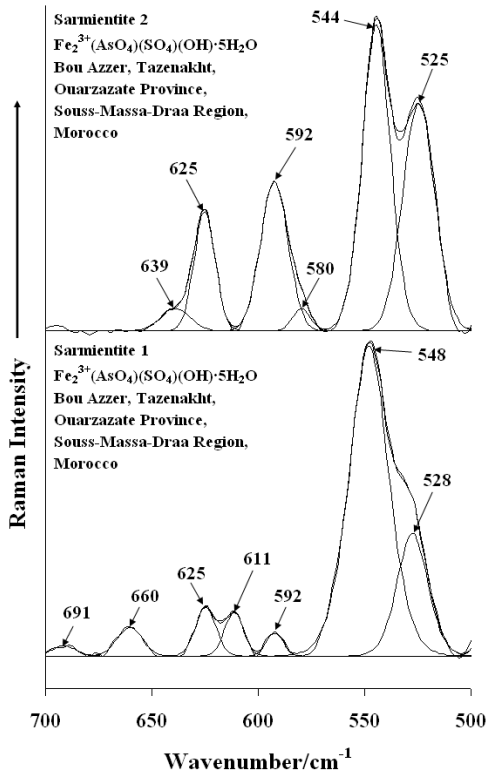

306

307

308 **Figure 7**

309

310

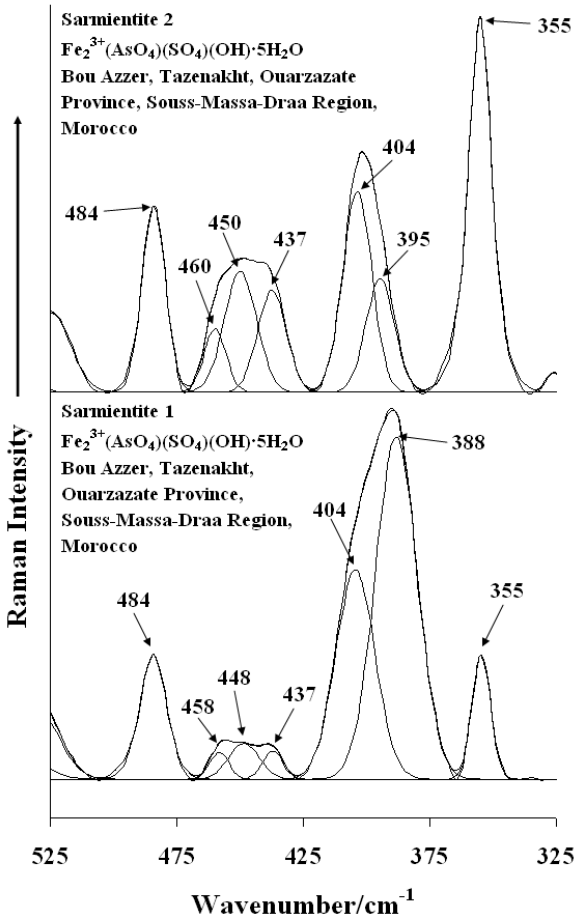

311

312

313 **Figure 8**

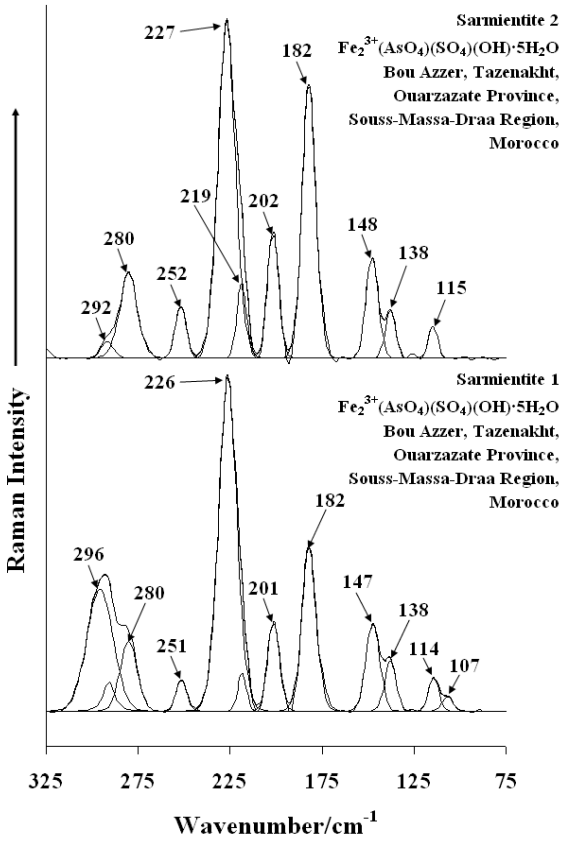

314

315 **Figure 9**

316

317

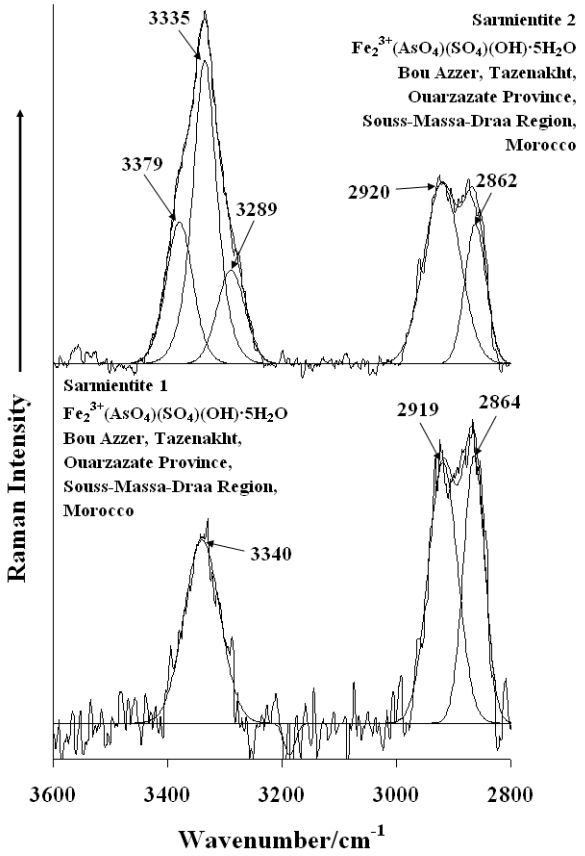

318

319

320 **Figure 10**

321

322

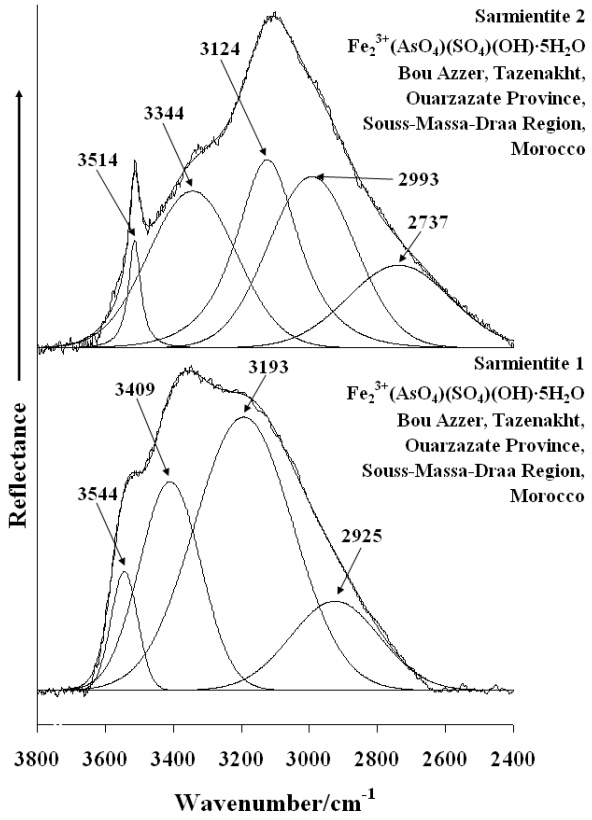
Sarmientite 2
$Fe_2^{3+}(AsO_4)(SO_4)(OH)\cdot 5H_2O$
Bou Azzer, Tazenakht,
Ouarzazate Province,
Souss-Massa-Draa Region,
Morocco
3514
3344
3124
2993
2737
Sarmientite 1
$Fe_2^{3+}(AsO_4)(SO_4)(OH)\cdot 5H_2O$
Bou Azzer, Tazenakht,
Ouarzazate Province,
Souss-Massa-Draa Region,
Morocco
3544
3409
3193
2925
Reflectance
3800 3600 3400 3200 3000 2800 2600 2400
Wavenumber/cm^{-1}

Figure 11